# The Role of Simulation in Long-rod Ricochet Phenomenon

**K. Daneshjou[1] and M. Shahravi[2]**
Mech. Eng. Dep't, Iran Univ. of Science and Tech.

## ABSTRACT
Ricochet of a tungsten long-rod projectile from oblique steel plates was investigated numerically, using two explicit finite element methods. These two methods are lagrange and SPH (smooth particle hydrodynamic). Critical ricochet angles were calculated for various impact velocities and strengths of the target plates in Lagrange and SPH methods. It was predicted that in both methods, the critical ricochet angle increases with decreasing the impact velocities and that higher ricochet angles were expected, if higher strength target materials were employed. The experimental results were compared with those predicted by the simulations and with the existing two-dimensional analytical model. Through investigation of the angles in which projectile only ricochets, both SPH and lagrange methods represent approximately, the same results. However, in the cases that projectile begins to crack in head region out of high impact angles, the SPH method yields better results. One other advantage of the SPH method is that no erosion occurs when using the SPH method. This means better satisfaction of the conservation of mass principle. Therefore, the correlation between the numerical and the available experimental data demonstrates that the SPH approach is a very accurate and effective analysis technique for long rod ricochet phenomena in ricochet of Tungsten rod with RHA target.

**Key Words:** Critical Ricochet Angle, Numerical Simulation, Smooth Particle Hydrodynamic, Lagrange Method

# نقش شبیه سازی در بررسی کمانه کردن گلوله‌های میله‌ای بلند

**کامران دانشجو و مجید شهروی**
دانشکده مهندسی مکانیک، دانشگاه علم و صنعت ایران

**(تاریخ دریافت: ۱۳۸۶/۷/۲۰؛ تاریخ پذیرش: ۱۳۸۷/۰۲/۲۰)**

## چکیده
در این مقاله، پدیده کمانه کردن پرتابه های میله‌ای بلند از جنس تنگستن در برخورد با اهداف مایل فلزی به وسیله دو روش المان محدود صریح: لاگرانژ[۳] و هیدرودینامیک مولکولی[۴]، مورد بررسی قرار گرفته است. زاویه بحرانی کمانه کردن به دست آمده از هر دو روش نشان می‌دهند که با افزایش سرعت برخورد یا افزایش مقاومت ماده هدف زاویه بحرانی کمانه کردن افزایش می‌یابد. نتایج حاصل از دو روش فوق با نتایج مدل‌های تحلیلی و تجربی مقایسه شده‌اند. در زوایایی از برخورد که پرتابه تنها کمانه می‌کند، هر دو روش لاگرانژ و هیدرودینامیک مولکولی نتیجه تقریباً یکسانی می‌دهند، ولی در زوایای نزدیکتر به زاویه بحرانی، کمانه کردن که پرتابه شروع به زخمی نمودن هدف می‌نماید، روش هیدرودینامیک مولکولی نتایج بهتری نسبت به روش لاگرانژ می‌دهد. یکی دیگر از مزایای روش هیدرودینامیک مولکولی نسبت به لاگرانژ این است که از اصل فرسایش پیروی نمی‌کند. لذا، قانون بقای جرم در حل مساله کاملا ارضاء می‌شود. در نتیجه، روش هیدرودینامیک مولکولی در شبیه‌سازی برخورد پرتابه‌های میله‌ای بلند با اهداف مایل نتایج دقیقتری نسبت به روش لاگرانژ می‌دهد.

**کلید واژه‌ها:** زاویه بحرانی کمانه کردن، شبیه‌سازی عددی، هیدرودینامیک مولکولی، متد لاگرانژ

1 - Professor: kdaneshjo@iust.ac.ir
2 - PhD Student (Corresponding Author): shahravi_d@yahoo.com
3 - Lagrange Method
4 - Smooth Particle Hydrodynamic Method (SPH)

**1- Introduction**

It is well known that a projectile impacting on a suitably inclined surface can bounce back from the surface or partially penetrate it (without perforating it and being stopped by it) along a curved trajectory on the impacted surface with a reduced velocity [1]. This phenomenon, known as ricochet, is controlled by such factors as properties of the materials constituting the projectiles and the impacted surfaces, impact velocity of the projectiles, and relative obliquity of the surfaces with respect to the impact path of the projectiles, etc [1].

Exploitation of ricochet to implement mass efficient means of amour protection is common in many military applications [2]. Despite numerous researches on ricochet of various types of projectiles from various types of surfaces, critical conditions for the ricochet of long-rod type projectiles has not been completely established yet. On the extension of the series of investigations on the impact of long-rods on targets [8-9], Tate first described ricochet using a simplified two-dimensional hydrodynamic model [3]. For the geometry shown in Fig. 1, it was predicted that ricochet of a projectile with a square cross section would occur if:

$$\tan^3\left(\frac{\pi}{2}-\theta\right) > \frac{2}{3}\frac{\rho_p v^2}{Y_p}\left(\frac{L}{D}+\frac{D}{L}\right)\left(1+\sqrt{\frac{\rho_p}{\rho_t}}\right) \qquad (1)$$

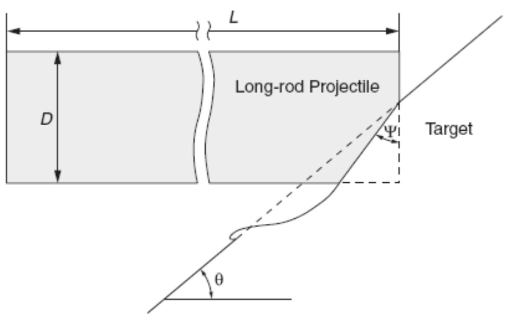


**Fig. (1):** Geometry used for two-dimensional analysis for ricochet of long-rod type projectiles by Tate [3] and Rosenberg *et al.* [4].

where, $\theta$ is the oblique angle, $\rho_p$ and $\rho_t$ are densities of the projectile and the target, respectively, $v$ is the impact velocity, $Yp$ is the dynamic strength of the projectile and $L$ and D are the length and diameter of the projectile, respectively. It is predicted from this expression that the higher projectile density, impact velocity and $L$ / D ratio and lower rod strength will result in a lower ricochet angle.

However, in the derivation of equation (1), it was assumed that the projectile is a rigid body and that ricochet occurs due to the rotation of the projectile around its mass centre caused by the asymmetric reaction force exerted on its front from the impacted surface. These assumptions do not properly reflect physical phenomena predicted and observed in real systems, where the projectile bends on impact and then a plastic hinge form, which travels backward with the progress of the projectile [1].

Rosenberg *et al.* [4] supplemented some of these shortcomings by further including the effect of target strength and bending of the projectile. The ricochet condition suggested by them is (see Fig. **1** for the geometry)

$$\tan^2\left(\frac{\pi}{2}-\theta\right) > \frac{\rho_p v^2}{R_t}\left(\frac{v+u}{v-u}\right), \qquad (2)$$

Where, $Rt$ is the dynamic yield strength of the target and $u$ is the penetration velocity which is expressed as [3]:

$$u = \frac{\rho_p v - \sqrt{\rho_p^2 v^2 - (\rho_p - \rho_t)\left\{\rho_p v^2 + 2(Y_p - R_t)\right\}}}{\rho_p - \rho_t}. \qquad (3)$$

Though the theoretical model developed by Rosenberg *et al.* includes the strength and density of both the target plate and the projectile, the $L$ / D ratio of the projectile and thickness of the target plate are excluded.

Recent numerical analysis by Zukas and Gaskill [6], suggested that two-dimensional plane strain analysis with FEM codes overestimates the critical ricochet angles and therefore should not be used for design purposes.

Thus, alternative approaches, use of experimental and numerical methods, have been used for more precise description of physical phenomena regarding ricochet by many researchers.

Reid *et al.* [7] carried out experiments on the deformation behavior of mild steel and aluminum long-rod projectiles striking at an undeformable oblique target and observed that the deformation of the projectiles consisted of impact end mushrooming and projectile buckling followed by its bending which terminated in a plastic hinge beyond which the projectile was not deformed.

Senf *et al.* [5] with a numerical work, predicted that the projectile bends on impacting the target plate and forms a plastic hinge which moves backward while its tip slides along the target surface. This prediction was supported by experimental observations. Some existing work on oblique impact [10-11] or near normal impact of the yawed projectiles [12-13] should also be noted. Although some useful information about the behavior of the projectile and target during high-velocity impact can be obtained from these studies, they are focused more on the penetration and perforation process rather than the ricochet phenomena and, in particular, critical ricochet conditions.

Especially, little attention has been paid to the numerical simulation capabilities and limitations in ricochet phenomena.

For structures under shock and impact loading, numerical simulations have proven to be extremely useful. They provide a rapid and less expensive way to evaluate new design ideas. Numerical simulation can supply quantitative and accurate details of stress, strain, and deformation fields that would be very expensive or difficult to reproduce experimentally.

The governing partial differential equations of simulated model need to be solved in both time and space domains. The solution over the space domain can be obtained utilizing different spatial discretizations such as Lagrange, Euler, ALE, or mesh-free methods.

Each of these techniques has several capabilities and limitations. Usually, there is not a single technique that is appropriate to all problems. In the present paper, Lagrange and SPH methods, are described and applied to investigate ricochet phenomena for oblique plate impacted by a projectile.

## 2- Numerical analysis

### 2.1- Methods of Space Discretization

The spatial discretization is performed by representing the fields and structures of the problem using computational points in space, usually connected with each other through computational grids. Usually, the finer the grid is, the more accurate the solution. The most commonly used spatial discretizations are Lagrange, Euler, ALE (Arbitrary Lagrange Euler - a mixture of Lagrange and Euler), and mesh-free methods such as SPH (Smooth Particles Hydrodynamics).

In many cases through solution of solid problems, Lagrange and SPH methods are employed, and most of the researches on long rod projectile and metallic target impact phenomenon are based on Lagrange method. This is because the Impact analyzing softwares are recently made capable of implementing the SPH technique. In this paper both methods are introduced and advantages and disadvantages of them through solution of ricochet problems are investigated.

### 2.2- Lagrange

The Lagrange method of space discretization, as described in [21], where the numerical grid moves and deforms with the material, is ideal for following the material motion and deformation in regions of relatively low distortion, and possibly large displacement. Conservation of mass is automatically satisfied and material boundaries are clearly defined. The Lagrange method is most appropriate for representing solids like structures and projectiles. The advantages of the Lagrange method are computational efficiency and ease of incorporating complex material models. The disadvantage of Lagrange is that the numerical grid can become severely distorted or tangled in an extremely deformed region, which can lead to adverse effects on the integration time step and accuracy. However, these problems can be overcome to a certain extent by applying numerical techniques such as erosion and rezoning.

Figure **2** shows a typical Lagrangian finite element model used in the numerical analysis. A general-purpose explicit finite element analysis package LS-Dyna was used for the numerical calculations. [15].

The model consists of a rectangular oblique target plate and a cylindrically shaped projectile with blunt nose shape that is initially located 1 mm away from the target. Only half of the whole geometry was modeled due to the inherent symmetry of the model along the x-direction of the coordinate as shown in Fig. **2**. The length and diameter of the projectiles chosen for the numerical analysis were 75 and 7 mm, respectively, giving an L/D of 10.7. Impact velocities of the projectiles were varied from 1000 to 2000 $m/s$ with an increment of 250 $m/s$. Target plates modeled are l50mm long, 40mm wide and 6.25 mm thick. Obliquity of the plates was varied from 3° to 25° with intervals of 1°. Typical eight-node linear brick elements with reduced integration were used for meshing as shown in Fig. **2**. Material properties were applied to the model by assigning appropriate material properties to the predefined projectile and target element sets, i.e. properties of WHA to the projectile element set and properties of the two types of high hardness steel, namely, RHA class 4 [14] and S-7 tool steel [15], to the target element set.

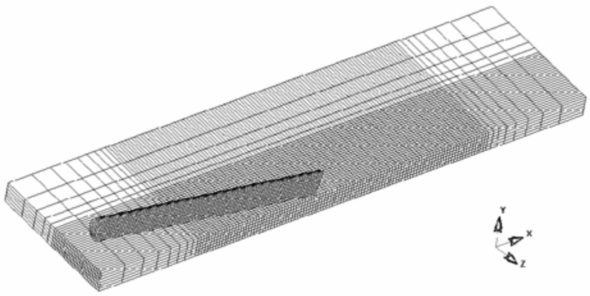


**Fig. (2):** Typical Lagrangian finite element mesh coordinate system used for the numerical study in this work.

In order to model a high-strain-rate mechanical response of the projectile and the target materials, a commonly used constitutive equation, the Johnson-Cook equation [15], was used as it is known to describe high-velocity mechanical response of a number of metals fairly well. This has the form:

$$\sigma = \left(\sigma_0 + B\varepsilon_p^n\right)\left(1 + CLn\frac{\dot{\varepsilon}}{\dot{\varepsilon}_0}\right)\left[1 - \left(\frac{T - T_r}{T_m - T_r}\right)^m\right], \quad (4)$$

where, $\sigma_0$ is the static yield strength, $\varepsilon_p$ the effective plastic strain, $\dot{\varepsilon}$ the effective strain rate, $\dot{\varepsilon}_0$ the reference strain rate, $T$ the temperature, $T_r$. The room temperature, $T_m$ the melting temperature and *B*, C, *m* and *n* are material constants. For the materials used in this study, these parameters were taken from Johnson and Cook paper. [15] and are shown in table **1** together with the basic physical properties required for the calculations.

Previous works indicates that using Mie-Gruneisen equation of state had provided good agreement between numerical and experimental results. Therefore, Mie-Gruneisen equation of state is used in my problem.

The Gruneisen equation of state with cubic shock velocity-particle velocity defines pressure for compressed material as:

$$p = \frac{\rho_0 C^2 \mu[1 + (1 + \frac{\gamma_0}{2})\mu - \frac{a}{2}\mu^2]}{1 - (S_1 - 1)\mu - S_2\frac{\mu^2}{\mu + 1} - S_3\frac{\mu^3}{(\mu + 1)^2}} + (\gamma_0 + \alpha\mu)E, \quad (5)$$

where, $E$ is the internal energy per initial volume, $C$ is the intercept of the $u_s - u_p$ curve, $S_1$, $S_2$ and $S_3$ are the coefficients of the slope of the $u_s - u_p$ curve, $\gamma_0$ is the Gruneisen gamma, and a is the first order volume correction to $\gamma_0$. Constants C, $S_1$, $S_2$, $S_3$, $\gamma_0$ and a are all input parameters. The compression is defined in terms of the relative volume, *V*, as:

$$\mu = \frac{1}{V} - 1. \quad (6)$$

For expanded materials as the pressure is defined by:

$$p = \rho_0 C^2\mu + (\gamma_0 + \alpha\mu)E. \quad (7)$$

Mie-Gruneisen parameters are shown in table **2**.

**Table (1):** Material properties and constants for the Johnson-Cook model applied to the numerical model.

| | WHA | RHA | S-7 |
|---|---|---|---|
| Shear modulus(GPa) | 152.02 | 76.96 | 79.96 |
| $\rho(kgm^{-3})$ | 17000 | 7840 | 7750 |
| Specific heat $(Jkg^{-1}K^{-1})$ | 134 | 477 | 477 |
| $T_m(K)$ | 1723 | 1809 | 1763 |
| $\sigma_0(MPa)$ | 1410 | 1160 | 1539 |
| $B(MPa)$ | 223.3 | 415.9 | 477 |
| n | 0.11 | 0.28 | 0.18 |
| C | 0.022 | 0.012 | 0.012 |
| m | 1.0 | 1.0 | 1.0 |

**Table (2):** Constants for the Mie-Gruneisen equation of state applied to the numerical model.

| | WHA | RHA | S-7 |
|---|---|---|---|
| $\rho_0(kgm^{-3})$ | 17000 | 7840 | 7750 |
| $C_0(km/s)$ | 3.85 | 4.61 | 4.57 |
| S | 1.44 | 1.73 | 1.49 |
| $\gamma_0$ | 1.58 | 1.67 | 2.17 |

The interaction between the projectile and the plate was simulated by a Lagrangian–Lagrangian contact algorithm based on a slave-grid/master segment concept. This algorithm checks eventual penetration of slave-grids through master segments and applies constant forces to push them back. Erosion of the projectile and the target was simulated through a so-called adaptive contact algorithm [17], which automatically updates contact definition between the interacting deformable bodies upon elimination of the elements when pre-set level of plastic strains, determined by a separate depth of penetration (DOP) calibration, are reached.

**2.3- Mesh-free Lagrangian Method – SPH (Smooth Particles Hydrodynamics)**

The mesh-free Lagrangian method of space discretization-SPH (Smooth Particles Hydrodynamics), initially was used in astro-physics [16]. SPH is a mesh-free method that can be applied to nonlinear problems with large deformation and large strains, especially for impact and penetration of solid structures. SPH holds promise to overcome many of the inherent limitations associated with classical Euler and Lagrange approaches. For example, severe mesh distortion is a typical difficulty evidenced with a classical Lagrangian solver for penetration problems. Such mesh distortion can result in inefficient small time steps as well as potentially inaccurate results. To alleviate mesh distortion, an erosion mechanism is sometimes introduced to remove highly distorted elements and thereby allow the calculation to continue. However, erosion techniques typically lack a physical basis and are primarily computational expedients to remove "bad" elements in order to simply continue the calculation. In an Eulerian approach, typically large regions of space must be meshed in order to model existing as well as future regions where material may flow. SPH, unlike Euler, does not need additional mesh to describe void regions into which material may flow. Thus, computational requirements are less than with Euler and similar to Lagrange. SPH may also be better than Euler to describe history dependent material behavior as the material remains with a given SPH node and is not advected nor "mixed" for multiple materials as in Euler. Thus, the SPH method has distinct potential advantages over the traditional Lagrange and Euler methods and is thus of increasing interest for solving non linear problems. By definition, there is no "mesh tangling" or "mesh degeneration" in the SPH solver. Moreover, a numerical erosion model is not needed. Therefore, the SPH method is very useful to simulate material behavior subject to severe deformation and distortion, for example, in hyper-velocity impact.

Therefore, in this section, numerical simulations were conducted employing an explicit finite element code with SPH solver.[21]

In SPH model, the equation of state is linear while the strength model is Von-Mises. The model is realized with 149600 particles for plate and with 6868 particles for projectile. Some previous tests have shown that 149600 particles are enough to represent the deformations of the plate during the perforation (Fig. **3** ).

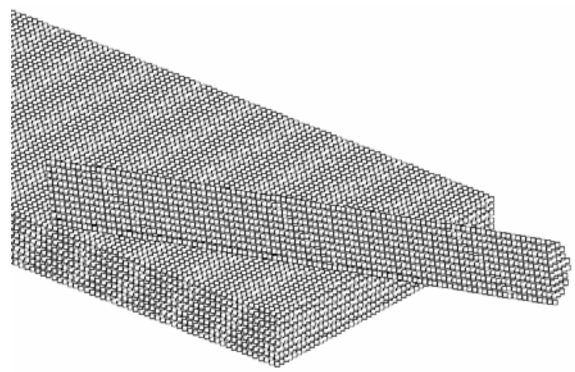

**Fig. (3):** SPH model used for the numerical study in this work.

**3- Experiments**

A series of ballistic experiments was carried out in last papers [22,23]. The experimental set-up shown in Fig. **4** consists of three witness blocks (38mm thick RHA class 4), an oblique target plate (6.25mm thick RHA class 4), a velocity-measuring device and a solid propellant gun. WHA projectiles with *L/D* ratios of 10.7 (*L* = 75 and *D* = 7 mm) were impacted at velocities of about 1000 and 1500ms−1. The velocities of the projectiles were controlled by adjusting the amount of solid propellant charge. The relations between the amount of the charge and the projectile velocities were calibrated in a preparatory experiment [22].

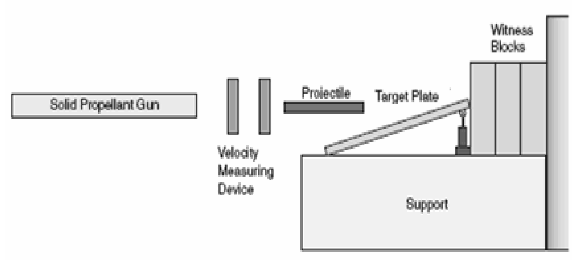


**Fig. (4):** Schematic illustration of the experimental set-up for the observations of oblique impact of long-rod projectile[22].

## 4- Results And Discussion

### 4.1- Post-impact Behavior of the Projectile and the Target Plate in Lagrangian Method

Numerical results are graphically shown in Fig's. **5-7** in terms of the mesh deformation with the lapse of time to analyze the behavior of the WHA projectile and the RHA target with thickness comparable to the projectile diameter during the oblique impact.

When the projectile impact velocity is 1000 $ms^{-1}$ and the target oblique angle is 10°, as in the case shown in Fig's. **5**, the projectile initially bends on impact (Fig. **5a**).

In the
the o

ricochet angle, the target does not deform much and no significant erosion of the impacted surface is noticed whilst the front end (denoted as head hereinafter) of the projectile lifts from the target surface after sliding some distance and eventually the projectile bounces away (Fig's. **5e-5h**). Such behavior is yielded due to the asymmetric reaction force exerted from the contact area to the projectile, which is reportedly proportional *to* the area *of* the contact, target strength and oblique angle [3-4, 7].

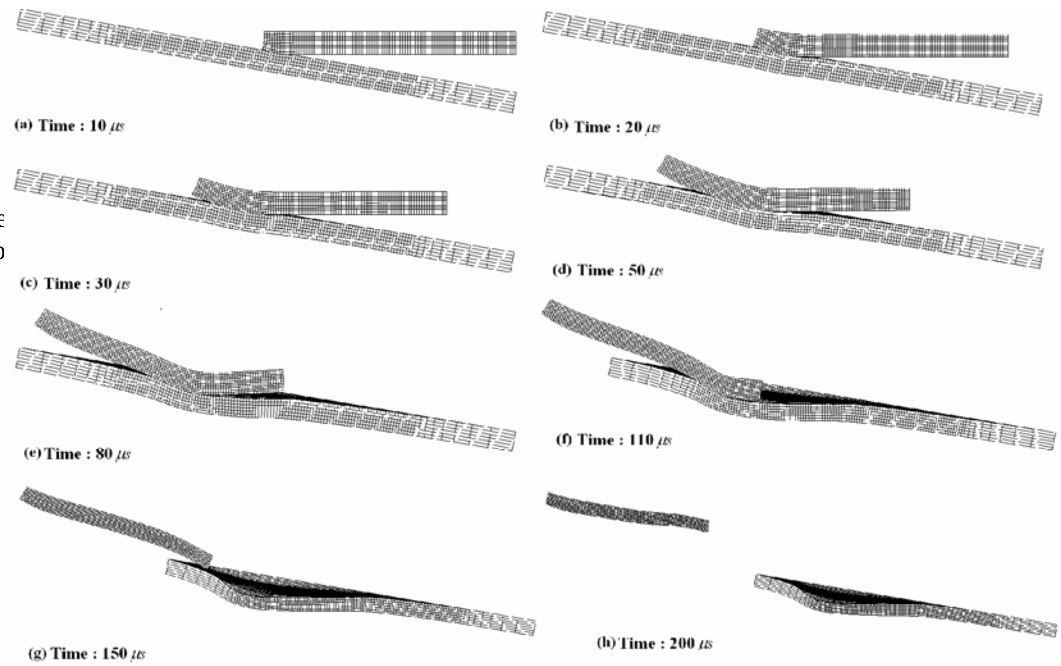


**Fig. (5):** Numerical results showing the behavior of the WHA projectile and the RHA target when the oblique angle is 10° and the impact velocity is 1000 m/s in Lagrange method.

When the oblique angle *of* the target plate is increased *to* 12° whilst keeping the impact velocity the same, the projectile shows somewhat different behavior. As shown in Fig's. **6a**-**6d**, it initially pushes the impacted area *of* the target inward following impact since the target plate is allowed. Whilst the head of the projectile tends to bounce back from the target due to the reaction force exerted from the contact area at the initial stage of the impact, its trailing portion (denoted as tail hereinafter) tends to penetrate into the target al.ong an almost identical trajectory of the initial impact (Fig. **6e**). Consequently, the front part ahead of the plastic hinge, which was bent and slid on the plate surface, bounces away whilst the rear part behind it penetrates into the deformed target forming a stretched section in the projectile and an impact crater in the target (Fig's. **6f** and **6g**). Indeed, the relatively thin deformable target plays a significant role in yielding such phenomena.

At the critical oblique angle, the tail also bounces away at a later time step before it completely perforates the target achieving critical ricochet (Fig. **6h**). At this stage the elongation of the projectile becomes so severe that it results in the fragmentation of the projectile.

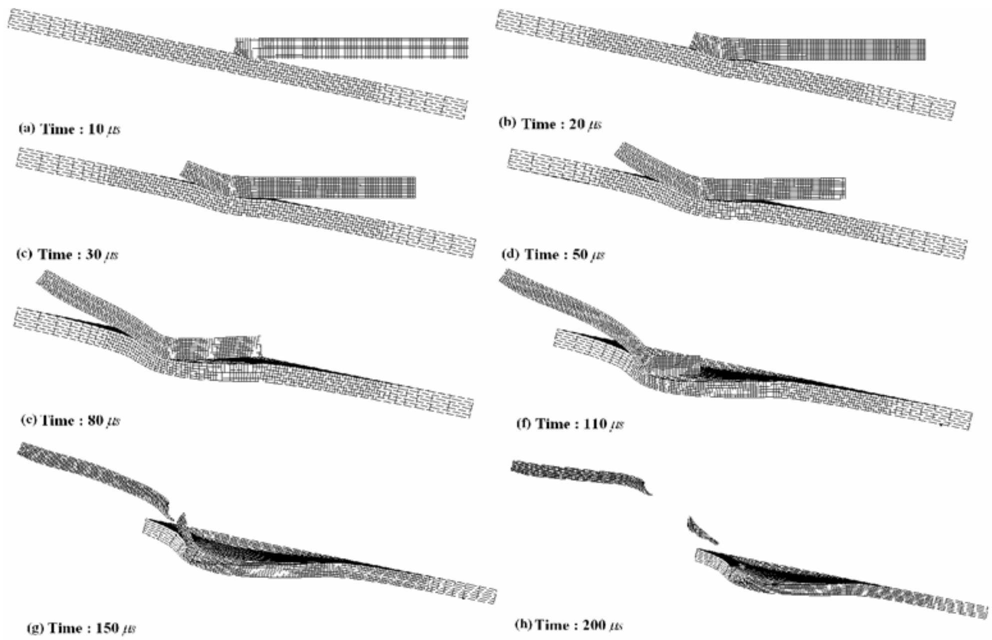


**Fig. (6):** Numerical results showing the behavior of the WHA projectile and the RHA target when the oblique angle is 12° and the impact velocity is 1000 m/s in Lagrange method.

In the case where the oblique angle is further increased *to* 14$^\circ$ beyond the critical angle, as can be seen in Fig's. **7a**-**7d**, the initial behavior *of* the projectile and the target is similar *to* the case *of* critical ricochet shown in Fig's. **6a**-**6d**.

However, unlike in the previous case, the tail part further progresses to penetrate into the target downward by eroding it (Fig's. **7e** and **7f** ), resulting in the fragmentation of the projectile due to extreme elongation as well as complete penetration (perforation) of the target as shown in Fig's. **7g** and **7h**.

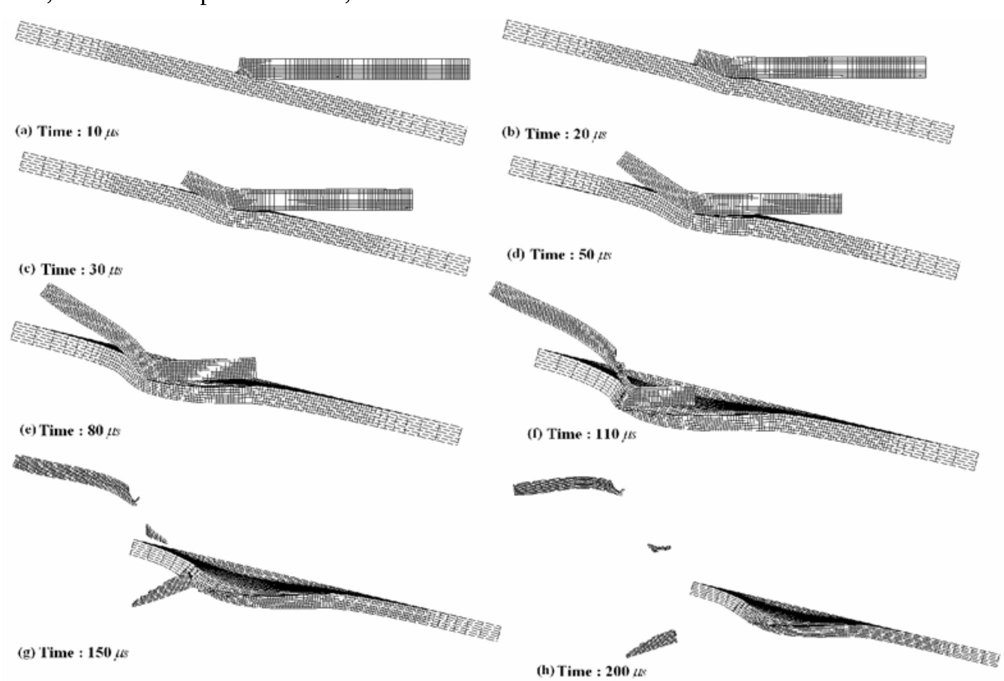


**Fig. (7):** Numerical results showing the behavior of the WHA projectile and the RHA target when the oblique angle is 14° and the impact velocity is 1000 m/s in Lagrange method.

Understanding the physical nature of the above behavior of the projectile and the target can be supplemented by analysing the changes in the projectile velocities after impact, as has also been performed for normal penetration in the literature [18-20]. For this purpose, post-impact changes in the horizontal (along the x-direction) and vertical (along the y-direction) velocities of head and tail of the projectile have been monitored during the numerical calculations and the results are plotted in Fig's. **8**-**13**. Before impact, the head and the tail move at the same initial velocity of 1000 ms$^{-1}$ and there is no vertical velocity term.

For the case with relatively low oblique angle, e.g. $\theta$ = 10°, as shown in Fig's. **8** and **9**, the horizontal velocities of the head and the tail of the projectile after impact are kept almost identical, implying no significant axial strain, which prevents the projectile segmentation. It can also be seen that the horizontal velocities did not decrease noticeably. From this, it is inferred that the projectile does not encounter any significant resistance to its motion along the flight trajectory and that the impact interaction of the projectile with the target does not cause any large-scale deformation of the target.

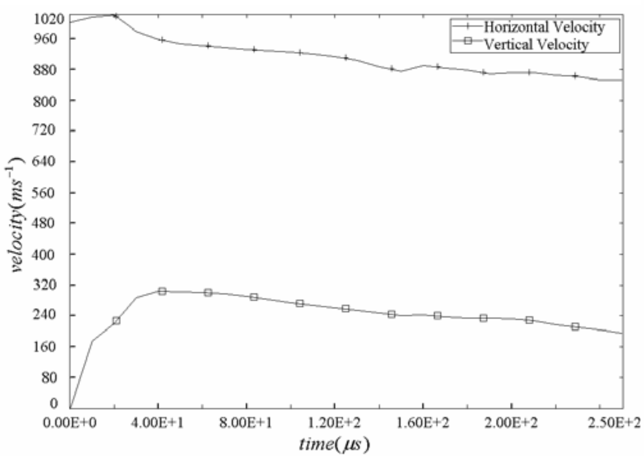


**Fig. (8):** Projectile head horizontal and vertical velocity ($\theta = 10^{\circ}$).

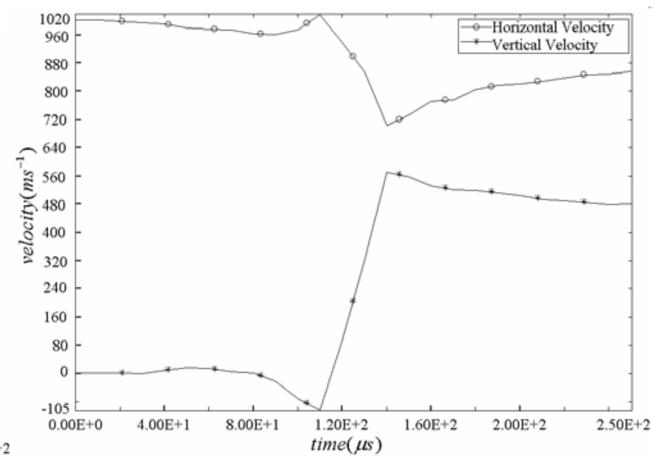


**Fig. (9):** Projectile tail horizontal and vertical velocity ($\theta = 10^{\circ}$).

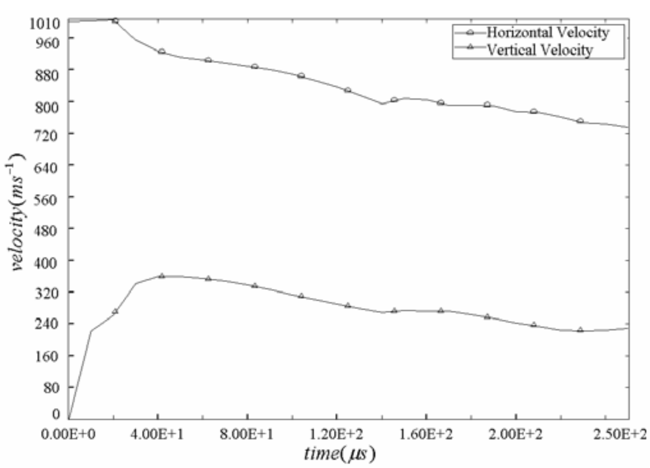


**Fig. (10):** Projectile head horizontal and vertical velocity ($\theta = 12^{\circ}$**).**

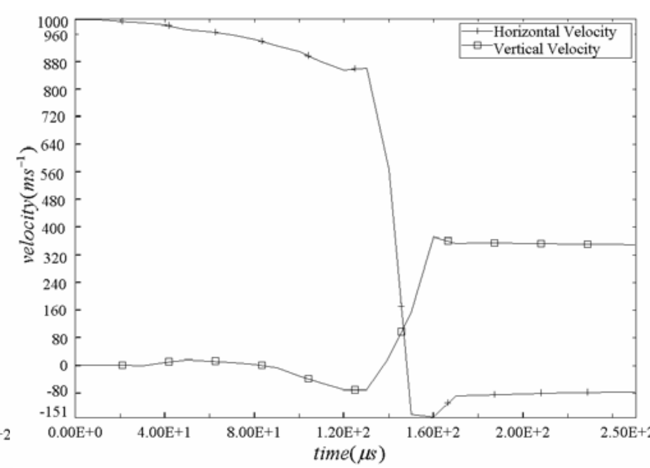


**Fig. (11):** Projectile tail horizontal and vertical velocity ($\theta = 12^{\circ}$).

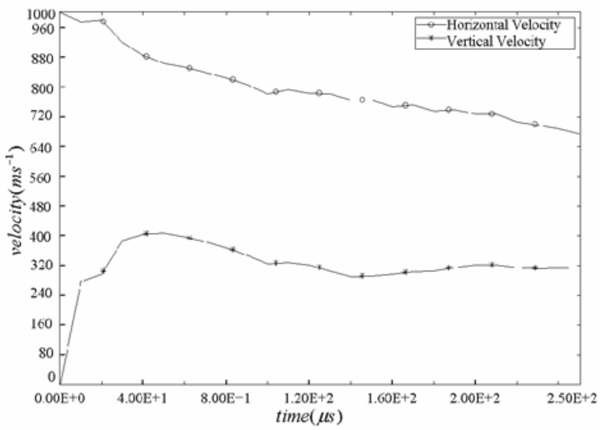


**Fig. (12):** Projectile head horizontal and vertical velocity ($\theta = 14^{\circ}$).

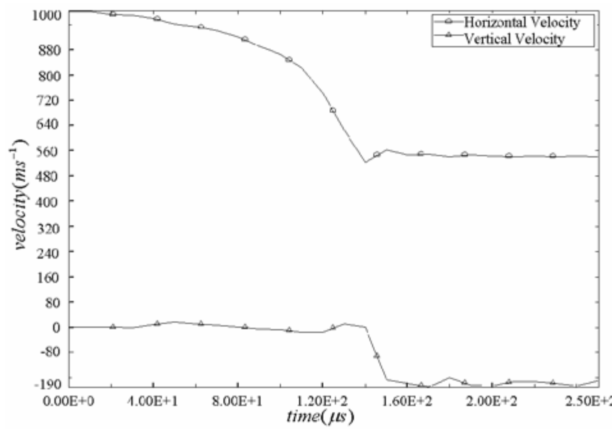


**Fig. (13):** Projectile tail horizontal and vertical velocity ($\theta = 14^{\circ}$).

Whilst there were only slight changes in the horizontal velocities, vertical velocities of the head and the tail undergo noticeable changes during the impact process. As can be seen in Fig. **10**, the vertical velocity of the head initially increases to about 300 ms $^{-1}$ and remains almost the same thereafter, which would be associated with sliding on the target surface and subsequent takeoff of the head shown in Fig. **5**. On the other hand, the vertical velocity of the tail is almost 0 until about 80 $\mu s$ and then increases to about 550 ms $^{-1}$ at 140 $\mu s$. This indicates that the impact of the head on the target does not cause any yawing force in the rear part of the projectile which is beyond the plastic hinge mentioned above. Near-constant vertical tail velocity of 460 ms-l after about 160 $\mu s$ would indicate the takeoff of the tail as shown in Fig's. **5f** and **5h**.

However, where critical ricochet was achieved ($\theta =$ 12° for the case considered herein), as shown in Fig. **10**, the decrease in the horizontal velocity of the head with respect to time is more pronounced than in the previous case, indicating that the progress of the head is hindered more. In particular, as shown in Fig. **11**, the horizontal velocity of the tail decreases to almost 0 from about 140 $\mu s$, producing a velocity difference between the head and the tail of about 750 ms $^{-1}$. Such a large velocity difference may cause large-scale deformation and therefore it would explain the stretching of the projectile shown in Fig. **6g** followed by the segmentation of the projectile shown in Fig. **6h**. At the same time, a sudden drop in the horizontal velocity of the tail between 100 and 150 $\mu s$ is believed to be related to the target cratering shown in Fig's. **6f** and **6g**, which could exert a high resistance to the advance of the tail. When critical ricochet is achieved, even though the impact crater is formed on the target, this does not lead to target perforation.

This can be explained from the changes in the vertical velocities of the head and the tail shown in Fig's. **10** and **11**, where it can be seen that the head and the tail sequentially acquire positive, vertical velocity components. They begin to take off from the target plate at about 0 and 150 $\mu s$, respectively, indicating no further penetration of the target.

A similar trend is obtained when the target oblique angle is further increased, e.g. $\theta$ = 14°, as shown in Fig's. **12-13** whilst two apparent differences are noticed.

First, the horizontal velocity of the head, once it is decreased to about 700 ms $^{-1}$ at about 120 $\mu s$, remains nearly constant implying that the flight of the head portion is no longer hindered by the target thereafter, probably due to the earlier segmentation of the projectile.

In the previous case shown in Fig. **10**, the head portion was connected to the tail portion through the elongated portion until the later time step so that the tail, still staying in the impact crater in the target, delayed the propagation of the head, which is represented as continuously decreasing velocity. Second, the behavior of the tail after segmentation is completely different: the vertical velocity of the tail decreases to a negative value of about -180 ms $^{-1}$ from about 150 ms $^{-1}$, which is then maintained almost constant after about 180 $\mu s$. This indicates that the fragmented tail is heading downward, which would be responsible for the perforation of the target shown in Fig. **7h**. The same as Lagrangian method results, SPH method results is shown in table **3**. Numerical results as shown in table **3**, describe **1** to **2** degrees difference between the critical ricochet angle achieved by SPH and Lagrange method.

In addition the table shows passing critical ricochet angle from higher to lower impact angles, the residual vertical velocity of the projectile changes sign.

**Table (3):** Projectile head and tail residual velocity results (SPH and Lagrange methods at 1000 m/s).

| Simulation method | $\theta$ (Degree) | Projectile head residual velocity (horizontal) | Projectile head residual velocity (vertical) | Projectile tail residual velocity (horizontal) | Projectile tail residual velocity (vertical) |
|---|---|---|---|---|---|
| Lagrange | 10 | 860 | 200 | 850 | 460 |
| Lagrange | 12 | 730 | 240 | -80 | 340 |
| Lagrange | 14 | 670 | 320 | 540 | -180 |
| SPH | 8 | 850 | 200 | 845 | 450 |
| SPH | 10 | 760 | 220 | -80 | 350 |
| SPH | 11 | 740 | 235 | 100 | -30 |
| SPH | 12 | 705 | 250 | 530 | -170 |
| SPH | 14 | 650 | 290 | 530 | -220 |

**4.2- Post-impact Behavior of the Projectile and the Target Plate in SPH Method**

Numerical results in SPH method are graphically shown in Fig's. **14-17**.comparing the Fig's. **14** and **15** with Fig. **5** shows many similarities, which confirms the prior claims about simulations using SPH technique.(Comparison between Fig's. **5a-5d** and **14a-14d** and **15a-15d**).

For example, in the case being considered ($\theta$ = 8$^\circ$), where the oblique angle is lower than the cri mu

surface is noticed whilst the front end (denoted as head hereinafter) of the projectile lifts from the target surface after sliding some distance and eventually the projectile bounces away (Fig's. **14e-14h**). Such behavior the same as last description is yielded due to the asymmetric reaction force exerted from the contact area to the projectile, which is reportedly proportional *to* the area *of* the contact, target strength and oblique angle.

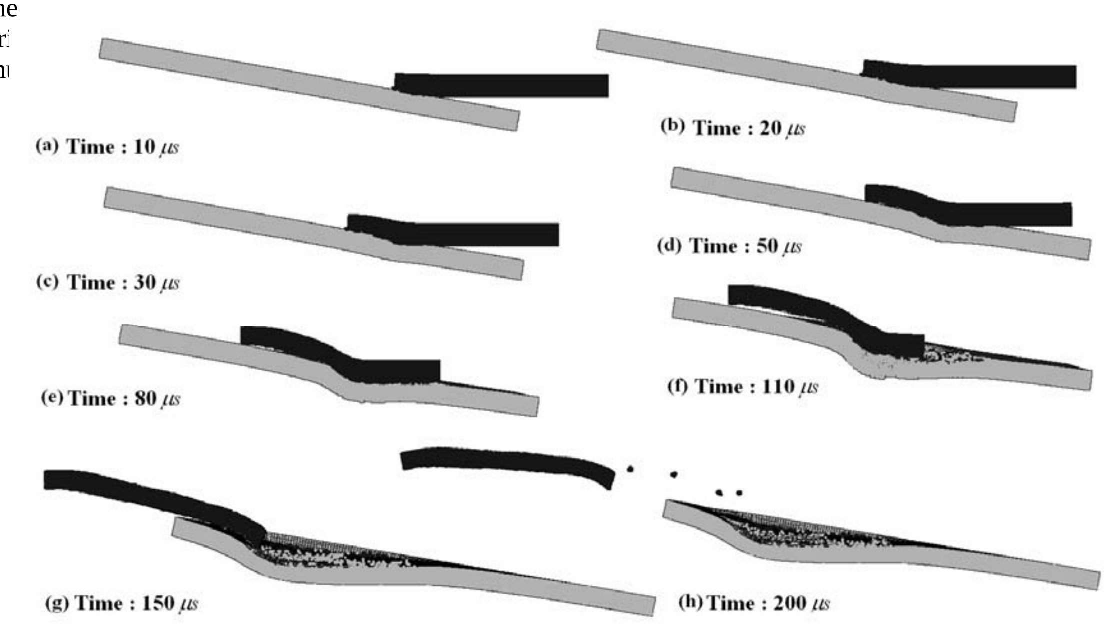


**Fig. (14):** Numerical results showing the behavior of the WHA projectile and the RHA target when the oblique angle is 8° and the impact velocity is 1000 m/s in SPH method.

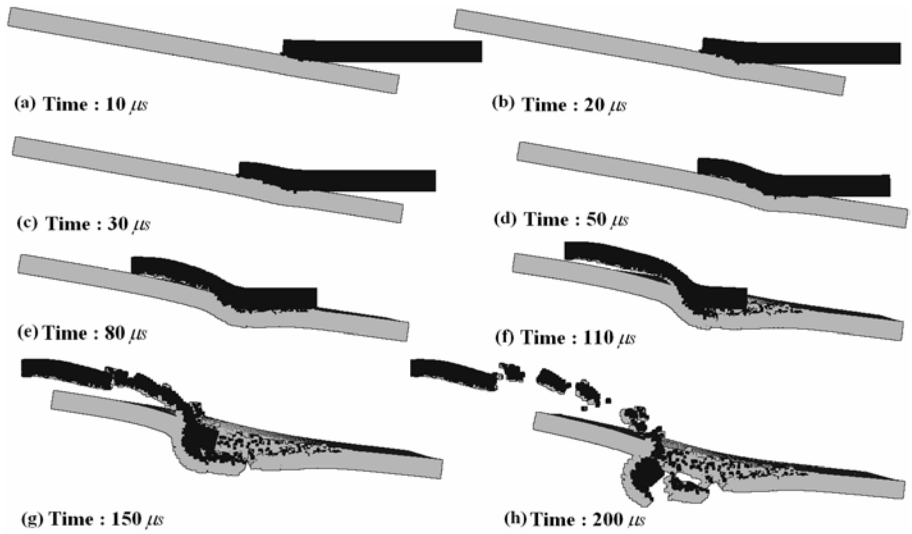


**Fig. (15):** Numerical results showing the behavior of the WHA projectile and the RHA target when the oblique angle is 11° and the impact velocity is 1000 m/s in SPH method.

When the oblique angle *of* the target plate in SPH method is increased *to* 10°, As shown in Fig's. **15a-15d**, it initially pushes the impacted area *of* the target inward following impact since the target plate is allowed.

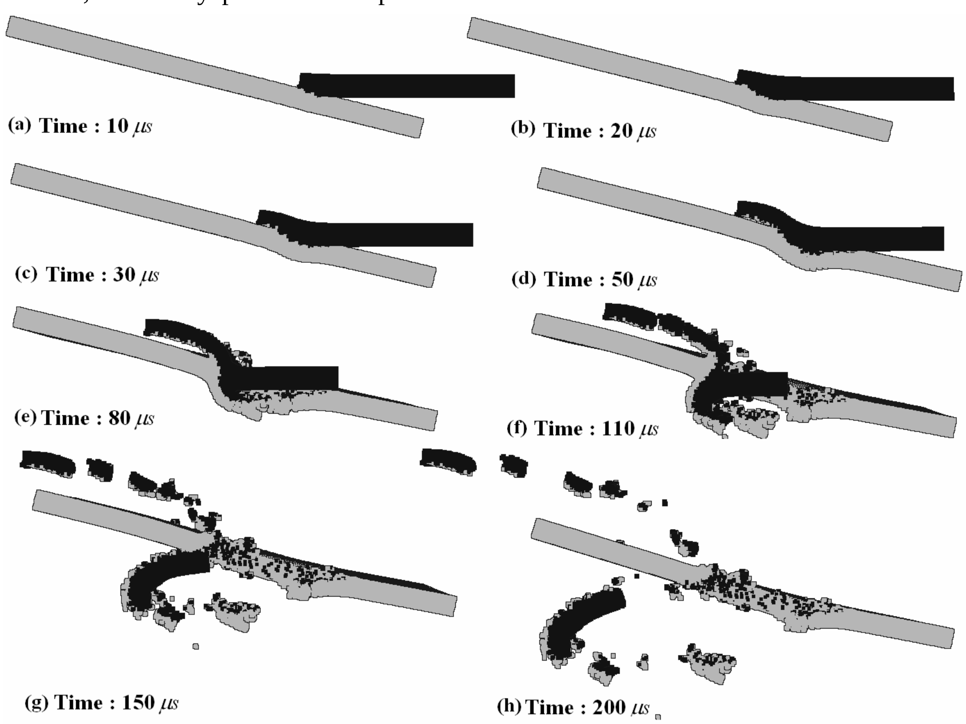


**Fig. (16):** Numerical results showing the behavior of the WHA projectile and the RHA target when the oblique angle is 12° and the impact velocity is 1000 m/s in SPH method.

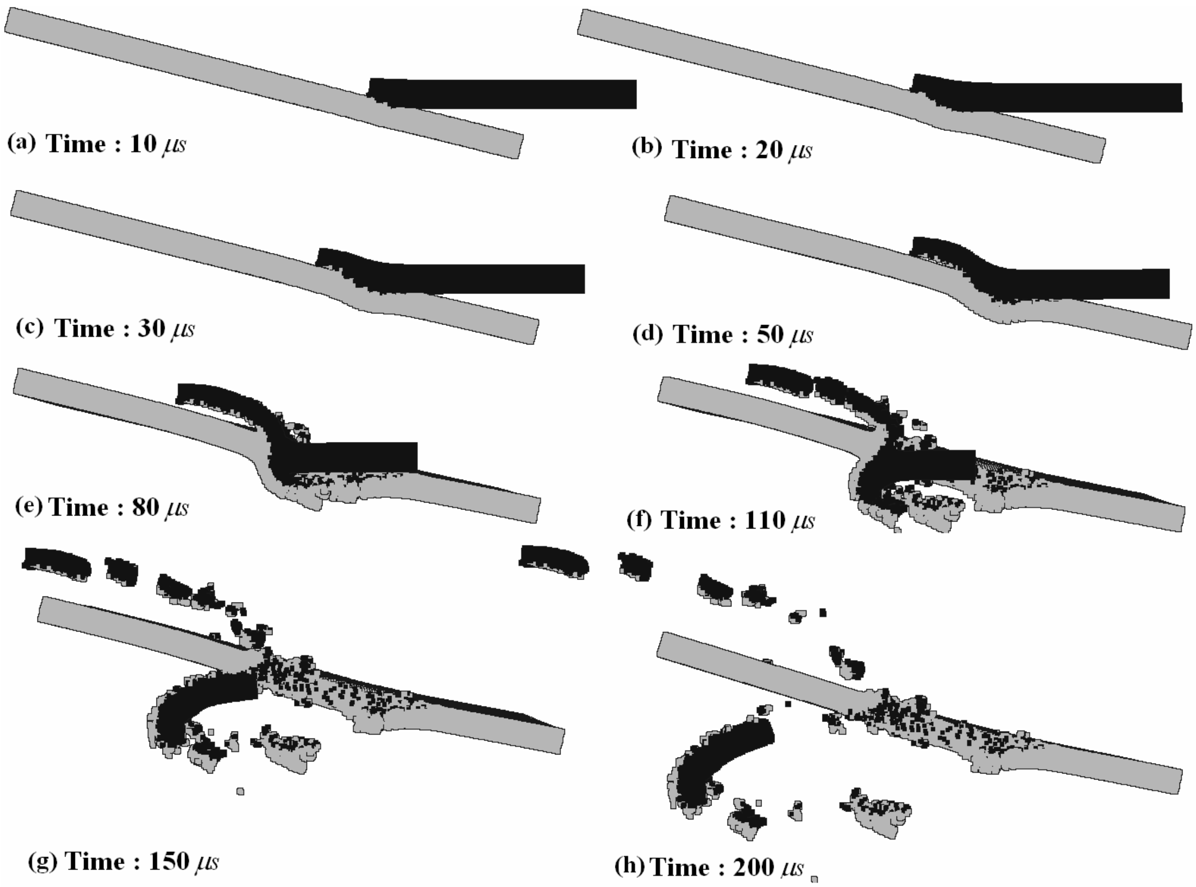


**Fig. (17):** Numerical results showing the behavior of the WHA projectile and the RHA target when the oblique angle is 14° and the impact velocity is 1000 m/s in SPH method.

In the case where the oblique angle is further increased to 12° and 14° beyond the critical angle, as can be seen in Fig's. **16a-16d** and **17a-17d**, the initial behavior of the projectile and the target is similar to the case of critical ricochet shown in Fig's. **14a-14d** and **15a-15d**.
From comparison between the Fig. **5** and Fig. **14**, also Fig. **6** and **15** and finally Fig's. **7** and **16**, it is readily seen that there is close coincidence between each pair. So it is concluded that the impact and deformation behavior of the projectile and the target derived from SPH in a certain angle is exactly in comply with the solution from Lagrange method but for an angel 1 to 2 degree more.

In accordance with the definition of ricochet mentioned in the introduction, changes in the critical ricochet angles were derived by analyzing the numerical results graphically in the manner described in two last sections, and were plotted as functions of impact velocities in Fig. **18** for the RHA target plate.

The ricochet angle curves shown in Fig. **18** were obtained from curve-fitting the numerical results as a first-order exponential decay function. The fitted equations, their parameter values, and the statistical analysis of the fitted results are also reported in the figure. The numerical results are confirmed with experimental results as shown in Fig. **18**. In this Figure the solid star markers indicate perforation of the RHA target plate by the long-rod projectile whilst the hollow circle markers indicate critical ricochet of the projectile.

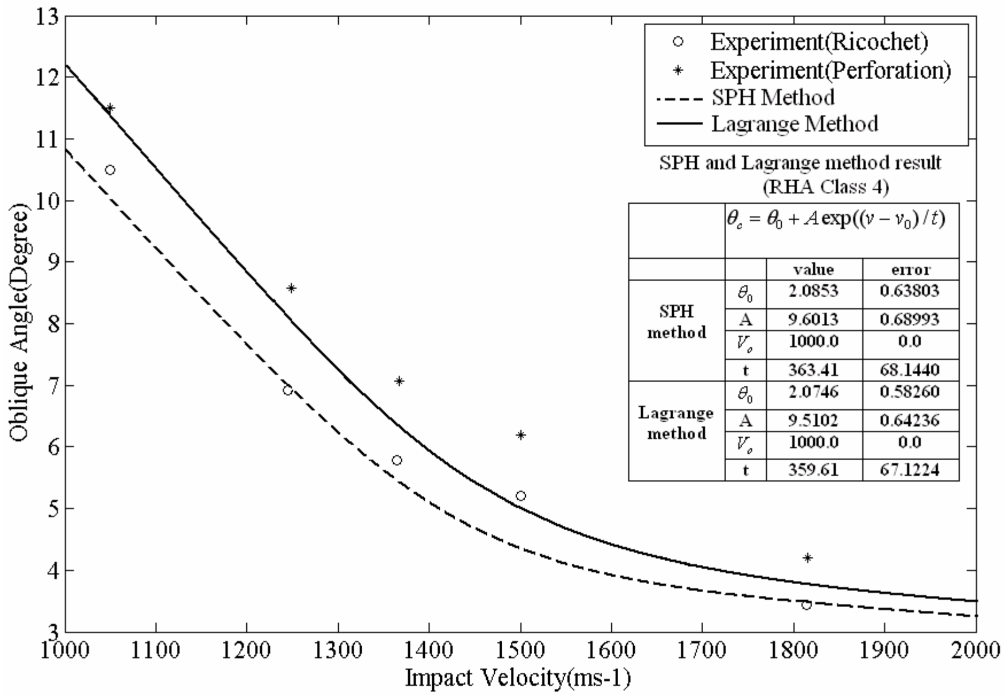

**Fig. (18):** Critical ricochet angles calculated by SPH and Lagrange.

Considering the above diagram for instance, we can say that according to Lagrange method the critical ricochet angle for impact velocity of 1000m/s is almost 12° where according to SPH solution this angle is extracted 11°. This means there is a difference of 1 to 2 degrees between the SPH calculated critical ricochet angle and the Lagrange one.

This difference comes up from the fact that erosion is not taken into account in SPH method and therefore the principle of conservation of mass is better satisfied. As a result none of the particles is omitted and the energy is completely applied to the target. This leads to penetration into target in lower angles, compared with the Lagrange method.

It can be seen that there is good agreement between the SPH results and test results for ricochet rather than Lagrange method.

Figures **19** and **20** compares the x-ray radiograph and simulations (Lagrange method and SPH method) of test .

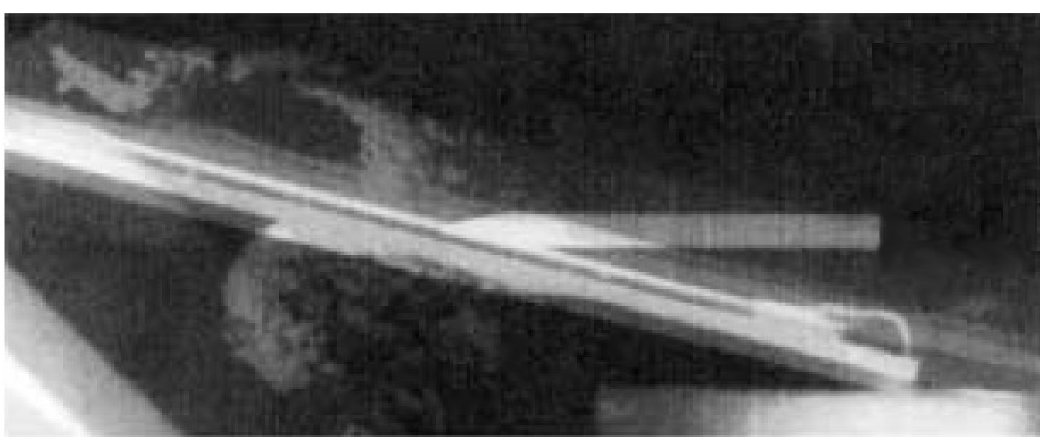
**Fig. (19):** Flash X-Ray of a test in $t = 100\mu s$ [23].

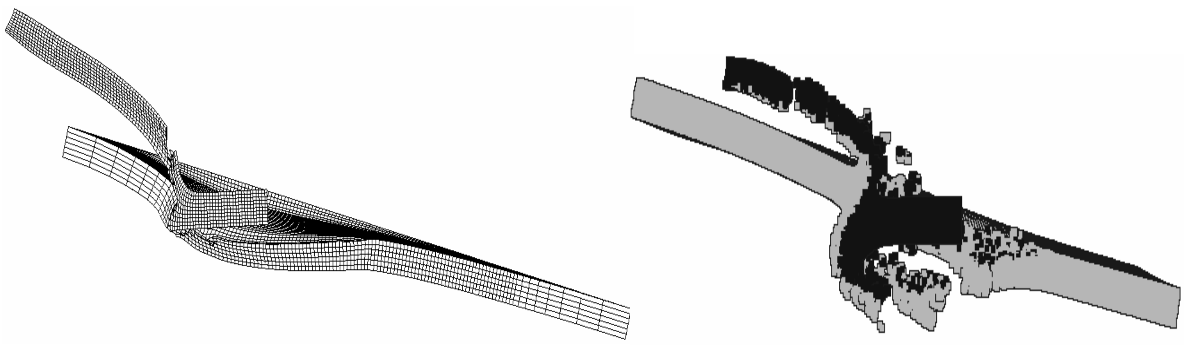

a) Lagrange Model b) SPH Model

**Fig. (20):** The simulation of projectile and target plate by SPH and Lagrange methods $\theta = 14^{\circ}$ , $t = 100\mu s$ .

In SPH method, the rod head ricochets while the tip stays intact and the rest of the front part shattered into a spray of particles. In SPH and Lagrangian method it is shown that central part of the rod perforates the target plate while eroded and deflected downwards relative to the rear surface of the plate. The tail of the rod keeps moving undisturbed in its original direction in every two simulation.

Examining the numerical simulation in SPH method results it was found that at the moment of impact the inclined plate pushes up the rod nose and a small crater is being created in the plate. This process ends after few tens of microseconds, after a small section of the front part of the rod is eroded and moves upwards. The amount of rod mass being pushed upwards in this test is about 27% of the overall rod mass. As the penetration proceeds, the eroded rod mass is moving forward because of its higher density. The non-uniformity of the crater in the target that has a finite thickness causes this debris to be pushed downwards and to emerge from the backside of the plate with a sideward velocity component. The amount of projectile mass that move downward at the moment the analysis was taken (100 μsec) is about 8–9 % of the rod mass. Generally speaking, there was always better agreement between the test results and SPH method rather than the Lagrange method, so it is concluded that SPH is a better procedure for simulation of the impact to oblique plates.

### 4.3- Compaction of the Analytical and Numerical Models

In this section the numerical results on the critical ricochet angles are compared with existing two-dimensional analytical models developed by Tate [3] and Rosenberg *et al.* [4], independently. The critical ricochet angles based on these models have been calculated for a WHA long-rod projectile and a RHA target as functions of impact velocities in Fig. **21**. Also shown are the corresponding numerical results. It can be seen in the figure that the Tate model overestimates the critical ricochet angle for impact velocities higher than 1170 ms−1 and *vice versa* for lower velocities. Further, the slope of Tate and Rosenberg curve are different from the Lagrange numerical results. On the other hand, the model developed by Rosenberg *et al.* shows a similar trend to the SPH numerical results; though the former overestimates the critical ricochet angles at all impact velocities. However, if it is shifted vertically downward in Fig. **21**, Rosenberg et al.'s model coincides closely with the numerical results and therefore their analytical model can be used as a practically useful guideline to estimate ricochet angles if used with care. Therefore here in the job, the SPH is known as the best tool to exact solution for 3D simulation impact problems.

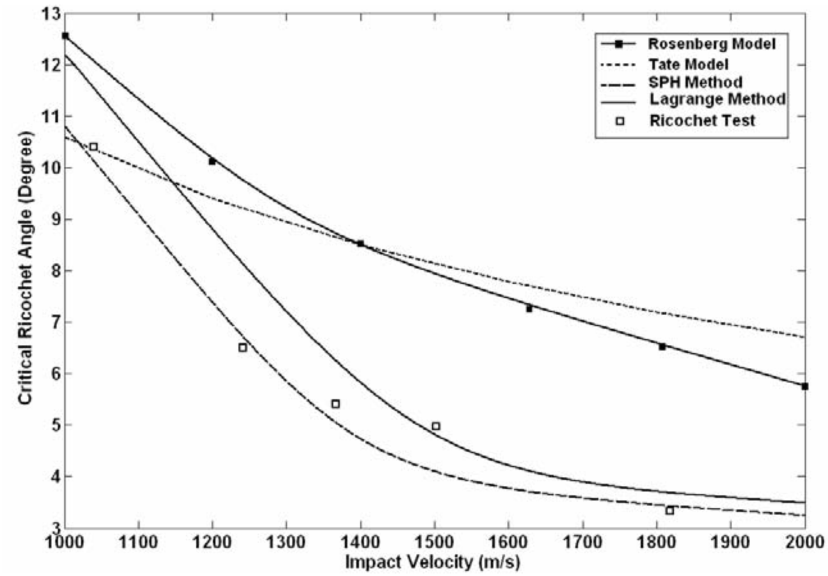


**Fig. (21):** Test result, SPH and Lagrange solutions, analytical models of Tate and Rosenberg.

**4.4- The Residual Length of the Projectile**

One other difference between the two methods is that, in SPH the projectile is shattered into relatively more particles than Lagrange method. Fig. **22** shows the length relation of the remaining particles for the two methods in impact angle of 14˚, which is $\frac{L1}{L1^{'}} = 0.5$ and $\frac{L2}{L2^{'}} \approx 1.$

Based on the test results (Fig. **19**) and several simulations, it is concluded that for the case of high impact angles (more than 12˚) and brittle projectile that is more probable to crack; the SPH technique represent better results compared with Lagrange method.

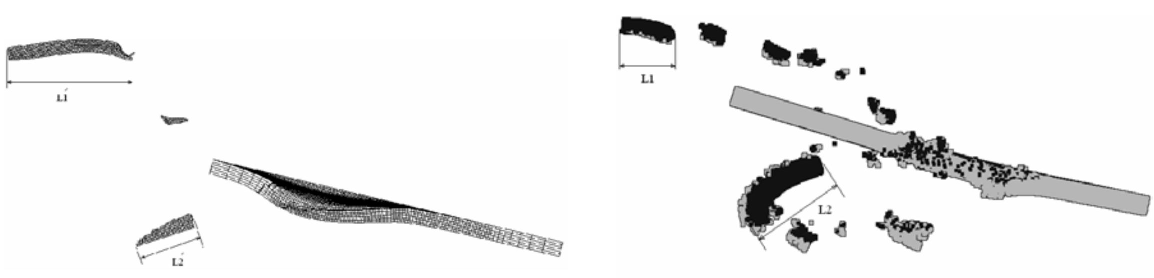


a) Lagrange Model b) SPH Model

**Fig. (22):** Residual length of the projectile in SPH and Lagrange methods.

The reason behind loss of small particles in Lagrange method is that the highly deformed elements are omitted out of erosion principle, so that the explicit code solution continues on.

One other difference between the two simulation techniques is shorter remaining particles after impact in SPH than Lagrange. This is because of more shattered and scattered particles in SPH than Lagrange method. Fig. **16** shows this difference.

**4.5- Target Plate Shape After Penetration**

One more disparity in these simulations is the difference in the form of rupture caused on the target plate. In Fig. **23** it is depicted that the SPH method simulates the impact effect and rupture in the target plate in more detail. This difference is also out of the eroded elements in highly deformed regions round the ruptured area.

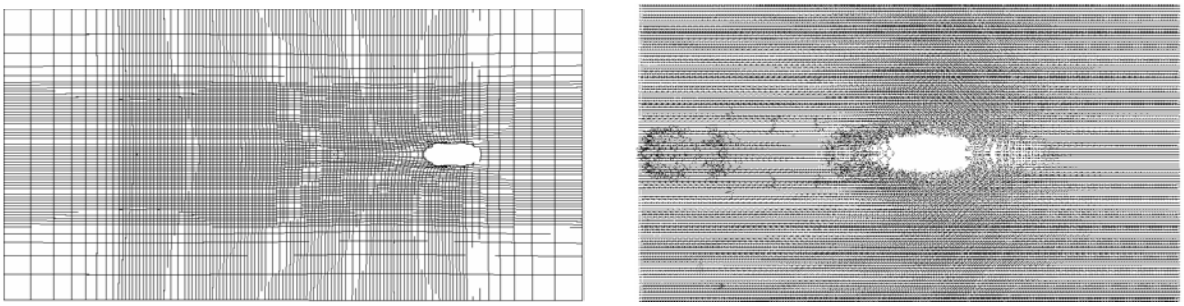


**Fig. (23):** Simulation of projectile and target plate by SPH and Lagrange in 200 $\mu s$ .

**4.6- Effects of the Target Strength**

Whilst the RHA has been widely used as a primary amour material over decades, in some cases, stronger material such as high hardness amour (HHA) has also been adopted, though its use is limited due to lower toughness. To investigate the effect of material strength on the ricochet angle, material constant terms in the Johnson–Cook model for S-7 tool steel, which has static yield strength and hardness similar to HHA produced by Thyssen Krupp AG, were taken from the literature [15] and applied to the numerical model. The ricochet angles calculated for S-7 tool steel were plotted as a function of the impact velocity in Fig. **24**. Numerical results have been curve-fitted using first-order exponential decay function as in the case of RHA. It can be seen that a higher ricochet angle is predicted for a given impact velocity if the target strength is increased.

Thus, at a given impact velocity, use of the high hardness plate, S-7 tool steel, would foster the ricochet of the projectile, i.e. the target plate can tolerate more vertical component of the projectile movement. This implies that the target plate with higher strength allows a higher oblique angle for the ricochet of the projectile at a given velocity.

It is further noticed in Fig. **17** that there is a salient increase in the ricochet angle especially at low impact velocities as the material strength increases whilst improvement in ricochet capability through the use of stronger materials gradually decreases at higher velocities.

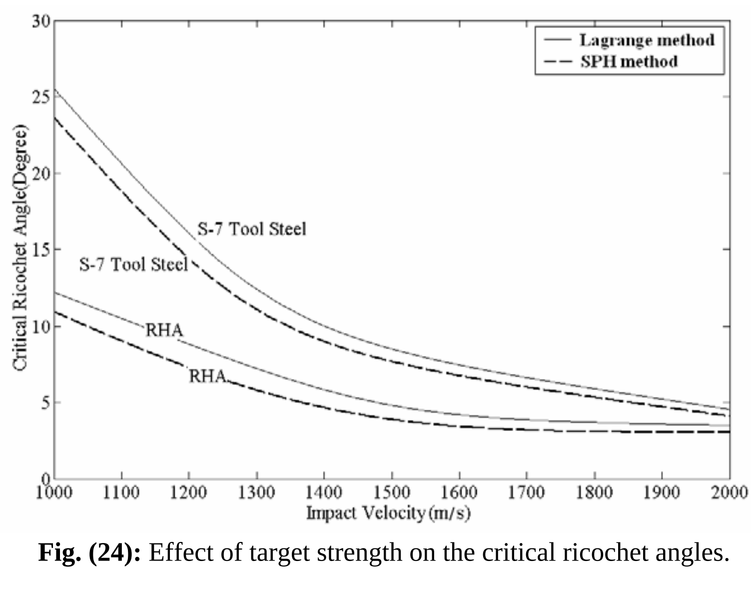


**Fig. (24):** Effect of target strength on the critical ricochet angles.

**5- Summary and Conclusions**

Ricochet of a WHA long-rod projectile impacting on oblique steel target plates with finite thickness was investigated numerically.
With SPH and Lagrange method three major phases of the interaction process were observed. In SPH method the rod head ricochets while shattered into a spray of particles. The central part of the rod perforates the target plate while being eroded and deflected downwards. The tail of the rod keeps moving forward almost undisturbed. In Lagrange method three phases are observed as well, but in the contrary the rod head does not shatter and only bends. According to test results, the tungsten rod head at high impact velocities shatters into a spray of particles.

Effects of the impact velocities of the projectiles and the hardness of the plates on the critical ricochet angle were considered.
Critical ricochet angles were also derived from the SPH numerical analysis and Lagrangian analysis. For the cases considered herein, the numerical study predicted that the critical oblique angle of the target plates required for ricochet of long-rod type projectiles rises with lower projectile velocity in two methods. But the SPH method prediction was shown to be more reliable by experimental results than Lagrange.
When the target hardness was considered, the numerical results predicted that a higher ricochet angle can be obtained by employing harder target materials for a given impact velocity, which was appreciable at lower velocities in particular.

If the only evaluation criterion was based on the angles lower than ricochet angle of the projectile, both lagrangian and SPH methods used here would be convenient for simulating ricochet phenomena. However, if all angles in this problem is essential evaluation point, with experimental trials data, the SPH seems to be more suitable.

**Refrences**


1. Zukas, J.A., “High Velocity Impact Dynamics”, John Wiley & Sons, Toronto, 1990.
2. Ogorkiewicz, R.M., “Technology of Tanks” (Coulsdon: Janes's Information Group), 1991.
3. Tate, A. “A Simple Estimate of the Minimum Target Obliquity Required for the Ricochet of a High speed Long rod Projectile”, J. Phys. D, Appl. Phys. Vol. 12, No. 5, p. 1825, 1979.
4. Rosenberg, Z., Yeshurun, Y. and Mayseless, M., “On the. Ricochet of Long-rod projectiles” The 11th Int. Symp. Ballistics, p. 501, 1989.
5. Senf, H., Rothenhausler, H., Scharpf, F., Both, A., and Pfang, W. “Experimental and Numerical Investigation of the Ricocheting of Projectiles from Metallic surfaces”. The 6th Int. Symp. Ballistics, p. 510, 1981.
6. Zukas, J.A. and Gaskill, B., “Ricochet of Deforming Projectiles from Deforming Plates” Int. J. Impact Eng., Vol. 18, No. 1, p. 601, 1996.
7. Reid, S.R. , Edmonds, A.J., and Johnson, W., “ Bending of Long Steel and Aluminum Rods During end Impact with a Rigid Target”, J. Mech. Eng. Sci., Vol. 23, No. 2, p. 85, 1981.
8. Tate, A. “A Theory for the Deceleration of Long-rod after Impact”, J. Mech. Phys. Solids, Vol. 15, No. 1, p. 387, 1967
9. Tate, A., “Further Results in the Theory of Long-rod Penetration” J. Mech. Phys. Solids 17, No. 12, pp. 141-150, 1969.
10. Roecker, E. and Grabarek, C., “The Effect of Yaw and Pitch on Long Rod Penetration into Rolled Homogeneous Armor at Various Obliquities ” The 9th Int. Symp. Ballistics, Vol. 2, No. 2, pp. 467-473, 1986.
11. Pierazzo, E. and Melosh, H.J., “Understanding Oblique Impacts from Experiments, Observations, and Modeling” Ann. Rev. Earth Planet. Sci, Vol. 28, No. 1, pp. 141-167, 2000.
12. Hohler, V. and Stilp, A.J., “Interferometric Investigation of Rod Deceleration During Impact Process”, The 6th Int. Symp. Ballistics, p. 333, 1981.
13. Anderson, C.E., Bless, S.J., and Sharron, T.R., Satapathy Sand Normandia M.J., “Investigation of Yawed Impact into a Finite Target” AlP Conf., p. 925, 1998.
14. Meyers, M.A., “Dynamic Behavior of Materials”, John Wiley & Sons, New York, 1994.
15. Ls Dyna User's Manual Version 970. (Livermore Software Technology Corporation), 2007.
16. Gingold, R.A. and Monaghan J.J., “Smoothed Particle Hydrodynamics, Theory and Application to Non-spherical Stars”. Mon. Not. Roy. Astron. Soc., Vol. 181, No.1, pp. 375-389, 1977.
17. Ls Dyna Theory Manual version 970. (Livermore Software Technology Corporation), 2007.
18. Rosenberg, Z. and Dekel, E., “A Computational Study of the Relations Between Material Properties of Long-rod Penetrators and their Ballistic Performance”

Int. J. Impact Eng. Vol. 21, No. 2, pp. 283-296, 1998.
19. Anderson, C.E., Walker, J.D., Bless, S.J., and Partom, Y., “On the L/D Effect for Long-rod Penetrators” Int. J. Impact Eng., Vol. 18, No.1, pp. 247-264, 1996.
20. Anderson, C.E. and Walker, J.D., “An Examination of Long-rod Penetration”, The Int. J. Impact Eng., Vol. 11, No. 2, pp. 481-501, 1991.
21. Quan, X., Birnbaum, N.K., Cowler, M.S., and Gerber, B.I., “Numerical Simulation of Structural Deformation Under Shock and Impact Loads, Using a Coupled Multi-solver Approach”, The 5th Asia-pacific Conf. on Shock & Impact Loads on Structures, pp. 71-78, 2003.
22. Woong, L.H.J.L. and Hyunho, S., “Ricochet of a Tungsten Heavy Alloy Long-rod Projectile from Deformable Steel Plates”, Int. J. Appl. Phys., Vol. 35, No. 2, 2002.
23. Yaziv, D., Mayseless, M., and Reifen, Y., “The Penetration Process of Long-rods into Thin Metallic Targets at High Obliquity”, The 19th Int. Symp. of Ballistics, Interlaken, Suwitzerland, 2001.